Vibration-induced drop atomization and bursting

By A. J. JAMES[1], B. VUKASINOVIC[2], MARC K. SMITH[2]
AND A. GLEZER[2]

[1]Department of Aerospace Engineering and Mechanics, University of Minnesota, Minneapolis,
MN 55455, USA

[2]The George W. Woodruff School of Mechanical Engineering, Georgia Institute of Technology,
Atlanta, GA 30332-0405, USA

A liquid drop placed on a vibrating diaphragm will burst into a fine spray of smaller secondary droplets if it is driven at the proper frequency and amplitude. The process begins when capillary waves appear on the free surface of the drop and then grow in amplitude and complexity as the acceleration amplitude of the diaphragm is slowly increased from zero. When the acceleration of the diaphragm rises above a well-defined critical value, small secondary droplets begin to be ejected from the free-surface wave crests. Then, quite suddenly, the entire volume of the drop is ejected from the vibrating diaphragm in the form of a spray. This event is the result of an interaction between the fluid dynamical process of droplet ejection and the vibrational dynamics of the diaphragm. During droplet ejection, the effective mass of the drop–diaphragm system decreases and the resonance frequency of the system increases. If the initial forcing frequency is above the resonance frequency of the system, droplet ejection causes the system to move closer to resonance, which in turn causes more vigorous vibration and faster droplet ejection. This ultimately leads to drop bursting. In this paper, the basic phenomenon of vibration-induced drop atomization and drop bursting will be introduced, demonstrated, and characterized. Experimental results and a simple mathematical model of the process will be presented and used to explain the basic physics of the system.

1. Introduction

In this paper, a new method for the atomization of a liquid, called vibration-induced drop atomization (VIDA), is introduced and studied. In the simplest VIDA process, a liquid drop is placed on a thin, circular metal diaphragm that is excited to vibrate sinusoidally by an attached piezoelectric ceramic disk. As a result of these vibrations, stationary axisymmetric standing waves are induced on the drop surface. Above a critical value of the excitation amplitude, an instability of the drop free surface occurs in which subharmonic azimuthal free-surface waves appear. These waves grow in amplitude and complexity as the excitation amplitude is increased. When the excitation amplitude is increased beyond a second well-defined critical value small secondary droplets begin to be ejected from the wave crests. At this point, without any further change in the excitation amplitude, the droplet-ejection process intensifies until suddenly, sometimes within a half a second or so, the entire primary drop breaks into a spray of smaller (between one and two orders of magnitude) secondary

droplets directed away from the diaphragm. Under certain conditions droplet ejection occurs so rapidly that the primary drop appears to atomize instantaneously. This event is called *drop bursting*, as opposed to droplet ejection, which refers to the detachment of a single droplet from the free surface of the larger primary drop. Additional experiments by the current authors (unpublished) and by Yule & Al-Suleimani (2000) on a scaled-up model of ultrasonic liquid atomization have shown that small secondary droplets can be ejected from multiple sites on a thin liquid layer instead of a drop. This opens the possibility that a continuous spray of small droplets can be created as long as the liquid film is continually replenished. The present work, however, focuses exclusively on the atomization of a single drop.

Numerous investigations, both experimental and theoretical, on the vibration of liquid films and drops have been presented in the literature. However, the majority of this work is limited to the formation and dynamics of the resulting surface waves. The formation of waves on the surface of a liquid layer due to vertical vibration was first reported by Faraday (1831). Several authors have used linear stability theory to determine the threshold forcing amplitude required for wave formation on a liquid layer, such as Benjamin & Ursell (1954) and Kumar & Tuckerman (1994). The nonlinear dynamics of Faraday waves have been studied analytically by Nayfeh & Nayfeh (1990), Miles (1993), Decent & Craik (1995), and Zhang & Vinals (1997). Numerous experiments have been performed to characterize the response of Faraday waves to the forcing amplitude and frequency, such as Ciliberto & Gollub (1985), Edwards & Fauve (1994), and Jiang *et al.* (1996), for example. Giavedoni (1995) presented a nonlinear finite-element simulation of Faraday waves. For a basic reference on Faraday waves, see the review by Miles & Henderson (1990).

The *free oscillations* of a drop attached to a solid surface have been studied experimentally by DePaoli, Scott & Basaran (1992), numerically by Basaran & DePaoli (1994) and Gañán & Barrero (1990), and theoretically for inviscid drops by Strani & Sabetta (1984) and for viscous drops by Strani & Sabetta (1988). In these studies, the oscillatory mode shapes and resonance frequencies of the attached drop have been determined as a function of the various system parameters.

The *forced oscillation* of a drop attached to a solid surface has received less attention. The first experiments seem to be those of Rodot, Bisch & Lasek (1979). These researchers immersed a drop of one liquid attached to a solid cylindrical support into a second immiscible liquid of the same density in order to simulate zero-gravity conditions. They forced the drop by oscillating the support vertically. The largest displacement amplitude was 1 mm (no more than one-third of the radius of the cylindrical support) and the forcing frequency was always less than 10 Hz. This corresponds to driving accelerations no more than about $0.4\,g$ (where g is the acceleration due to gravity on Earth). Under these conditions, the authors observed the first five axisymmetric modes of drop oscillation and large drop deformations. They even reported droplet ejection in which the drop forms a neck near the support that ultimately breaks under some experimental conditions.

Wilkes & Basaran (1997) studied forced drop oscillations numerically using the finite-element method. In their model, a liquid drop is surrounded from above by a passive ambient gas and is forced by the vertical motion of a solid support. The displacement amplitudes used were less than or equal to 20% of the support radius and the largest dimensionless frequency was $\Omega = 15$. This corresponds to driving accelerations no more than about $13\,g$ (for a water drop on a support of radius 5 mm). These authors computed the first three modes of drop oscillation and also observed large drop deformations.

Very few researchers have investigated the use of forced excitation to create droplet ejection. Sorokin (1957) presented photographs of chaotic droplet ejection from a vertically vibrated water-filled vessel and determined the energy required for ejection. Woods & Lin (1995) reported atomization of a liquid layer into a micron-sized spray by means of a vibrating cantilevered beam. Goodridge *et al.* (1997) established a threshold acceleration for droplet ejection from a liquid layer in a vertically oscillating container. They concluded that the threshold acceleration depends only on surface tension and forcing frequency for low-viscosity fluids and only on viscosity and forcing frequency for high-viscosity fluids. Wilkes & Basaran (1998, 2001) extended the work of Wilkes & Basaran (1997), by increasing the forcing amplitude to the point where they observed the onset of droplet ejection at a critical dimensionless forcing amplitude of $A_c = 0.273$. They defined droplet ejection to be when the radius of the neck that forms is 0.2% of the support radius. One example from their latter work is a computation of a droplet ejection event for a set of parameters that corresponds to zero gravity and (for a water drop on a support of radius 5 mm) a driving frequency of 13.4 Hz, an amplitude of 1.37 mm, and an acceleration of 0.99 g (see their figure 8). Jiang, Perlin & Schultz (1998) generated steep standing two-dimensional Faraday waves in a rectangular tank at a fundamental frequency of 1.60 Hz. They showed that increasing the forcing amplitude produced a period-tripled wave-breaking behaviour related to a nonlinear interaction between the fundamental mode and its second temporal harmonic. They observed one wave profile occurring every third wave (their mode A) in which a steep wave produced an upward jet that broke to eject a cylindrical 'droplet'. The relationships between this previous work and the single-droplet ejection process observed in drop bursting will be explored in a future publication.

The possibility of atomization of a drop by means of induced vibrations was reported by Lee, Anilkumar & Wang (1991) in their study of acoustically levitated drops. They presented images of a drop being atomized on a vibrating diaphragm instead of being levitated, but they reported no other results on this effect. In Smith *et al.* (1998) the present authors first reported their observations of drop atomization and drop bursting. We also presented the mathematical model used in the present work and discussed some preliminary comparisons between experimental data and simulations using this model. Vukasinovic, Glezer & Smith (2000) used the same experimental apparatus as in the present work and showed a visualization of vibration-induced drop atomization of a sessile drop. In Vukasinovic, Glezer & Smith (2001), a sequence of transitions that were observed in the drop as the driving amplitude was increased from zero were shown. In these visualizations, we considered small-amplitude forcing on the order of 100 μm or less, but used forcing frequencies on the order of 1000 Hz. These conditions imply a maximum forcing acceleration on the order of 400 g. This combination of large forcing frequencies and accelerations enabled us to excite the higher modes observed in the drop. This is the key to producing multiple droplet ejection sites over the entire free surface of the primary drop. Also, it is these driving conditions that distinguish this work from the previous work on forced drop oscillations by Rodot *et al.* (1979) and Wilkes & Basaran (1997, 1998, 2001).

The present work will report both qualitative and quantitative data on vibration-induced drop atomization and bursting. The purpose is to document the physical nature and character of these processes. To this end, observations of the different kinds of instabilities, droplet ejection, and drop bursting for a water drop placed on a vibrating surface are presented in §2. In §3, the experimental apparatus and

protocols used are discussed. The experimental data that characterize the drop–diaphragm system response lead to a simple mathematical model that explains the drop-bursting process. The formulation of this model is presented in §4. In §5, results from the experiments and the model are presented and compared. The mathematical model is linearized in §6 to demonstrate the robust physics captured by this simple model. Finally, in §7, conclusions, some directions for future work, and other potential applications of drop bursting are discussed.

2. Drop bursting

Before the details of the experiment and the mathematical model are described, a few visualizations of drop bursting are presented in order to introduce this novel phenomenon. For each figure shown below, a 100 µl water drop was placed at the centre of a horizontal circular metal diaphragm. The diaphragm was clamped at its periphery and excited by a piezoelectric ceramic disk so that it vibrated in the vertical direction in its fundamental axisymmetric mode.

Figure 1 shows a sequence of video frames of a drop as the excitation amplitude is slowly increased and then held fixed for a long enough time for transient motions associated with the amplitude increase to die out. The frequency is fixed at 987 Hz. Figure 1(a) shows the unforced drop for reference. For small values of the excitation amplitude, axisymmetric standing waves exist on the free surface of the drop as shown in figure 1(b). These waves have the same frequency as the excitation and are present at even very small values of the excitation amplitude. Above a critical excitation amplitude, an azimuthal mode of instability is triggered along the contact line of the drop. This mode couples with the existing axisymmetric waves to produce an azimuthal high-wavenumber wave on the free surface of the drop (figure 1c). This wave is at first stationary, but then experimental imperfections cause it to slowly rotate along the periphery of the drop in either the clockwise or counterclockwise direction. This instability is also signalled by the appearance of a subharmonic frequency in the free-surface motion – the signature of a classic Faraday-wave instability. When the excitation amplitude is increased further, the free-surface waves increase in magnitude and complexity and become time dependent (figure 1d). The development of distinct craters and liquid spikes that are in continual time-dependent motion are shown in figure 1(e). Finally, figure 1(f) shows the initial phase of the bursting process.

The rate of droplet ejection depends on the excitation amplitude, but more interesting is the fact that for a fixed excitation amplitude the rate of droplet ejection may increase or decrease with time. When droplet ejection begins, wave motion and the droplet ejection sites seem to be evenly distributed over the entire free surface of the drop. The most interesting event, bursting, occurs at some finite time after the first appearance of droplet ejection. The length of this time interval depends on the excitation amplitude. When a large excitation signal is suddenly applied to the diaphragm, bursting occurs almost immediately. For smaller excitation amplitudes (but still large enough), bursting may be delayed by on the order of seconds to perhaps a minute or more after the forcing is applied. In some instances bursting does not occur at all, even though droplet ejection is present.

The sequence of images presented in figure 2 shows what happens when a step-function-modulated sinusoidal excitation signal with a prescribed frequency and amplitude is applied to the diaphragm. Note that all of the different modes of instability on the drop free surface described in the previous case are still present. There is the initiation of axisymmetric waves in figure 2(b), the growth of the
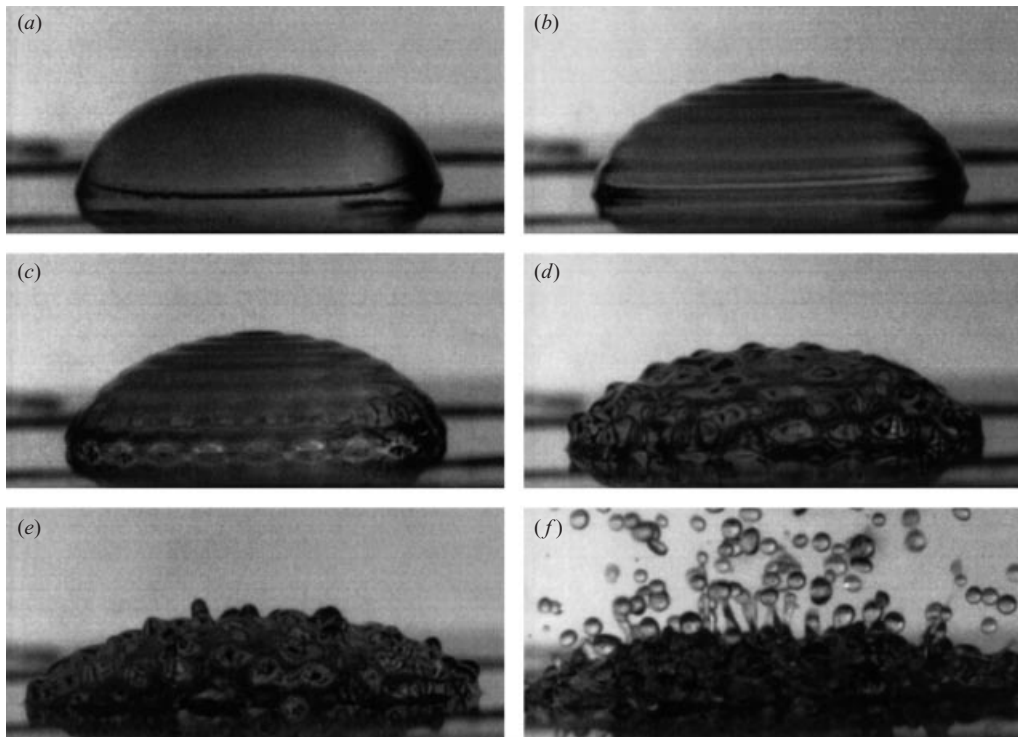
FIGURE 1. A sequence of video frames showing the side view of a 100 μl liquid drop (diameter ≈ 8 mm) on a diaphragm vibrating at 987 Hz. The excitation frequency is held fixed. The excitation amplitude is slowly increased from image (*a*) to image (*f*), and is held fixed for a long enough time for transient motions associated with the increase to die out before each image is taken. (*a*) The undisturbed drop, (*b*) axisymmetric standing waves on the free surface at small excitation amplitudes, (*c*) the appearance of stationary and then slowly rotating azimuthal waves on the free surface, (*d*) intense time-dependent wave motion over the entire drop free surface, (*e*) the appearance of time-dependent craters and liquid spikes, and (*f*) the rapid-ejection process of small secondary droplets (bursting).

azimuthal instability in figure 2(*c*), and the development of complex wave patterns and bursting in the remaining images. The time from the initiation of the excitation until the first secondary droplets are ejected is about 8 forcing periods (figure 2*d*). In real time, this is only 8 ms. Figure 2(*i*) is approximately when the entire primary drop is completely atomized. For this case, the bursting event took about 0.3 s.

Two close-up views of the free surface of a primary drop undergoing droplet ejection are shown in figure 3. The field of view of each picture is 3 × 3 mm. In (*a*), a liquid spike appears, grows, and then there is the appearance and growth of a secondary droplet on its tip that eventually pinches off with an upward velocity. In (*b*), a liquid spike appears with a droplet at its tip. The spike is shrinking, but the secondary droplet continues to form and eventually it pinches off, although this time it has a downward velocity. (This form of droplet ejection is in qualitative agreement with the computations of Wilkes & Basaran 1998, 2001.) In spite of the fact that the initial motion of the ejected droplet is toward the primary drop in this case, the secondary droplet and the primary drop may never coalesce. For low-viscosity fluids like water, secondary droplets usually bounce off the waves on the primary drop's free surface, and may continue to do so many times. The reason for this is that the time
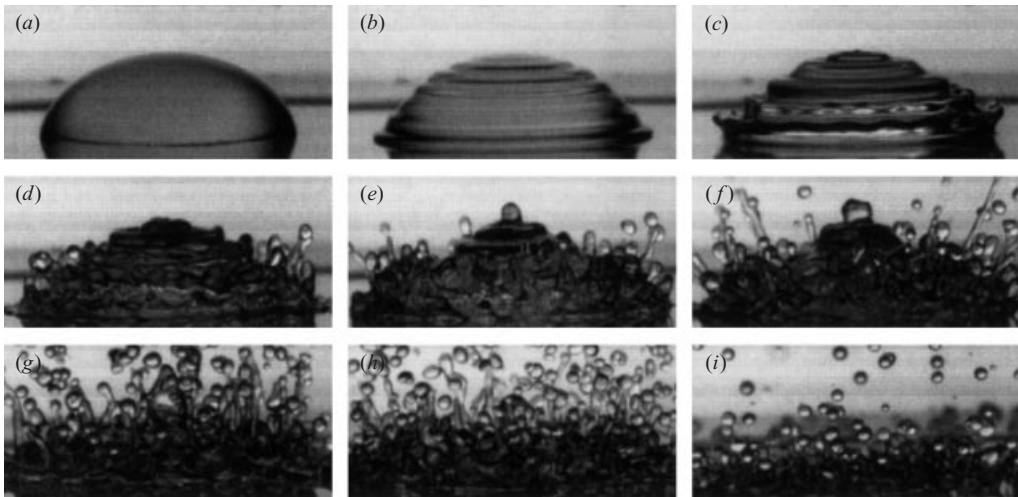
FIGURE 2. A time sequence of images of a 100 μl liquid drop (diameter ≈ 8 mm) on a vibrating diaphragm forced by a step-function-modulated sinusoidal excitation. The frequency (987 Hz) and the amplitude are fixed. (*a*) $t/T = 0$, (*b*) $t/T = 4.3$, (*c*) $t/T = 5.9$, (*d*) $t/T = 8.1$, (*e*) $t/T = 9.2$, (*f*) $t/T = 10.3$, (*g*) $t/T = 14.6$, (*h*) $t/T = 16.2$, (*i*) $t/T = 273.8$. Here, t is the time and $T \approx 1$ ms is the forcing period.
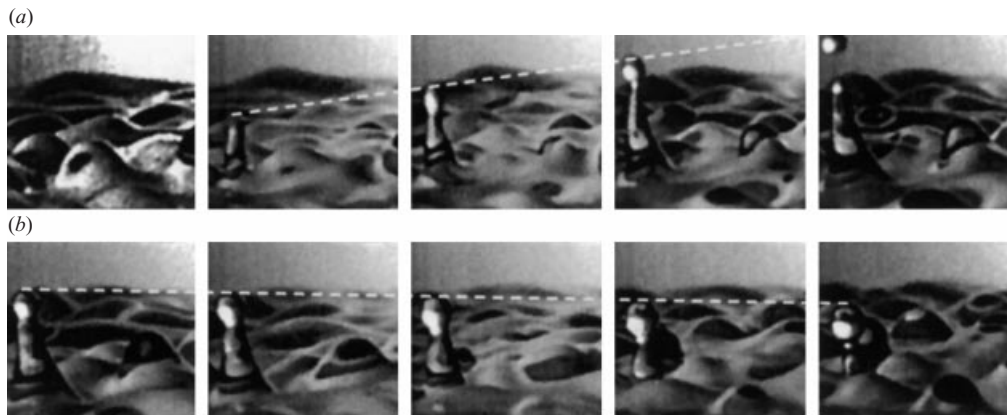

FIGURE 3. Two sequences of single droplet ejection from the free surface of a primary drop. The frequency (987 Hz) and amplitude of the excitation are held constant. The field of view is 3×3 mm. In (*a*), the ejected droplet has a velocity away from the primary drop; in (*b*), the ejected droplet has a velocity toward the primary drop.

scale for the rupture of the gas film between a secondary droplet and the primary drop is much larger than the time scale (≈ 1 ms) for the motion of the waves on the free surface of the primary drop. Thus, the secondary droplet continues to bounce off the primary drop's wavy free surface until it either reaches the surface of the diaphragm or until it finally coalesces with the primary drop.

When droplet ejection begins (and even just before this state), the wave motion on the free surface of the primary drop appears to be mostly chaotic. Thus, any single ejection event is not the result of a steadily growing free surface wave that eventually terminates in droplet ejection. Figure 4 shows the best time-resolved sequence of images for a full droplet ejection event, given the constraint of the video-frame-
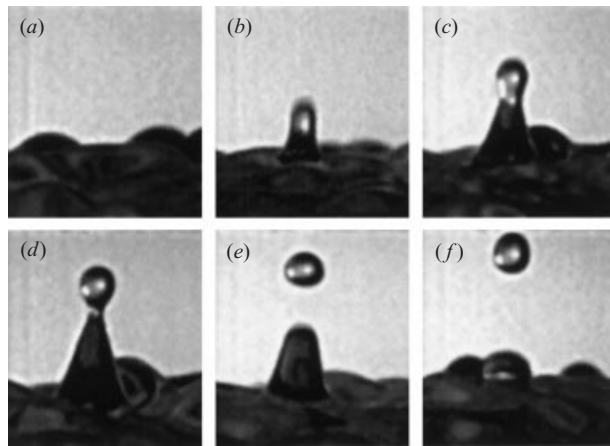
FIGURE 4. A time sequence of images taken at 3000 fr/s of a single secondary droplet ejection event from a drop forced at 987 Hz with a constant excitation amplitude. The field of view is 2×2 mm. The total time span of the sequence is 1.4 forcing periods (≈ 1.4 ms).

sampling rate. During the chaotic wave motion on the free surface of the primary drop a depression, or crater, precedes the rising liquid spike that ultimately ejects the secondary droplet. This is similar to the spike observed after the collapse of a cavity caused by an air bubble that has just broken through the free surface of a liquid layer from below, as presented in the work of Newitt, Dombrowski & Knelman (1954), and later by Snyder & Reitz (1998).

Another phenomenon to which bursting can be compared is the impact of a drop on a solid surface or a liquid layer. In either case a crater is formed, followed by a jet that may eject several secondary droplets. A particularly famous example is shown in the beautiful strobe-lit photograph of a splashing milk drop by Edgerton & Killian (1939). Fukai *et al.* (1995) presented an experimental and numerical study of the evolution of a drop impacting a solid surface. Pumphrey & Crum (1988) and Pumphrey, Crum & Bjørnø (1989) presented images of a liquid drop impacting a tank full of liquid. They were primarily interested in the underwater sound caused by air bubbles that sometimes form, but their images show the formation of a crater that is sometimes followed by a jet that ejects secondary droplets. They note that when the impact velocity is large enough, 'the resulting collapsing air cavity often ejects drops back into the air' (Pumphrey & Crum 1988). Additionally, one of their images (figure 5g, Pumphrey *et al.* 1989) is strikingly similar to figure 4(*d*). It shows a conical spike with a spherical drop on the end. Oğuz & Prosperetti (1990) presented numerical simulations of the experiments of Pumphrey & Crum (1988) and Pumphrey *et al.* (1989) using a boundary-element method. Their work verified that the formation of a crater may result in a droplet-ejecting jet.

Formation of a crater also seems to be important in the present work. This event may be a necessary condition in order for the resulting wave crest, or jet, to have sufficient momentum to eject a secondary droplet and to propel it away from the primary drop. Further study of this structure and its behaviour is presented in a companion paper, James, Smith & Glezer (2003).

Two contrasting cases of secondary droplet ejection with approximately the same level of forcing are presented in figure 5. In figure 5(*a*), there is the short conical spike with a large droplet forming on its tip that was also shown in figure 4. Figure 5(*b*), however, shows a spike that looks like a fluid jet undergoing a Rayleigh capillary
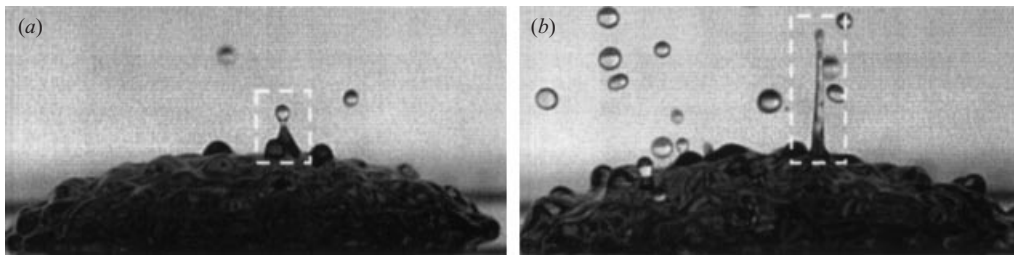
FIGURE 5. Two distinctive secondary-droplet ejections. (*a*) A large droplet forming at the tip of a conical spike, and (*b*) the initial stages of small-droplet formation as a result of a Rayleigh capillary instability of a liquid jet.

instability in addition to having a small droplet forming at its tip. In this case, the jet usually develops into several droplets resulting in multiple secondary-droplet ejections.

With this introduction to VIDA and drop bursting, the goal for the remainder of this paper is to explain and characterize the bursting events seen in figures 1 and 2. In the sections that follow, quantitative results from several experiments and from a simple mathematical model of the bursting process will be presented. Identifying and characterizing the mechanism of a single secondary-droplet-ejection event, as shown in figures 3–5, is considered in James *et al.* (2003).

3. Experimental setup

The experimental setup for this work is shown in figure 6. The transducer used to vibrate the liquid drop was a circular iron–nickel diaphragm 32 mm in diameter and 0.1 mm thick. A piezoelectric ceramic (PZT, 20 mm diameter, 0.12 mm thickness) was plated onto a small circular area centred on the lower surface of the diaphragm to create a unimorph structure. The diaphragm was mounted in an aluminium ring holder by clamping the outer edge with a retaining ring. The inside diameter of this ring and thus the active diameter of the vibrating diaphragm was 30 mm. The diaphragm was excited using a signal generator coupled to an amplifier that applied a sinusoidal voltage to the piezoelectric ceramic. This caused the ceramic to expand and contract, which induced the diaphragm to vibrate in its fundamental axisymmetric mode. The frequency and voltage applied to the piezoelectric ceramic were monitored and controlled. For the experiments discussed in § 5, the forcing voltage was turned on instantaneously using a step-function modulation of the amplitude. In the diaphragm characterization studies of § 4, the voltage amplitude was held fixed at each frequency.

Because of its low mass the mechanical resonance frequency of the transducer is around 1 kHz and it is capable of providing extremely large accelerations. The present transducer is capable of delivering maximum accelerations up to 1000 *g*. However, to prevent accidental damage to the transducer, the maximum acceleration in almost all experiments conducted in the present work was limited to less than 350 *g*, which corresponds to a displacement magnitude of less than 90 µm. Besides the magnitude of acceleration, the present transducer differs from conventional shakers in its spatial variation of the forcing imposed on a drop (the acceleration ranges from zero at the edge of the diaphragm to a maximum at the centre). For a 200 µl water drop (the drop volume used in the bursting experiments reported in § 5), the acceleration varies by 22% from the centre of the drop to the contact line, while for a 100 µl water drop (the drop volume used in the visualization studies shown in § 2), the variation is only 15%.
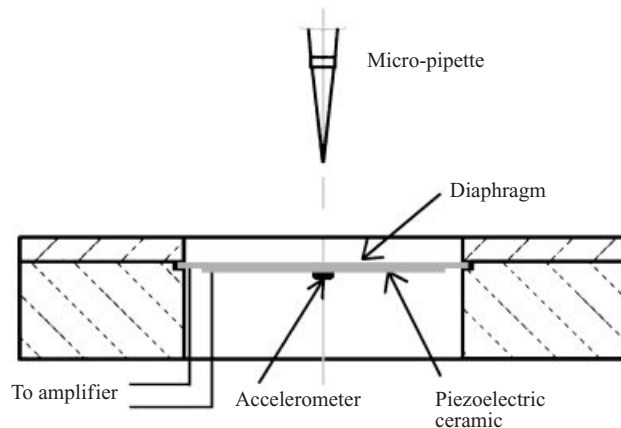
FIGURE 6. A sketch of the experimental setup for the VIDA and drop-bursting experiments.

The acceleration of the diaphragm was measured using a microfabricated accelerometer (Endevco 25A) glued to the centre of the piezoelectric ceramic on the lower surface of the diaphragm. The accelerometer had a range of $350\,g$ and a precision of $\pm 0.2\,g$. Given a fixed forcing frequency, nominally about $1\,\text{kHz}$, only the oscillation amplitude of the output from the accelerometer was recorded. This amplitude was obtained with a small electrical circuit that squared and low-pass-filtered ($40\,\text{Hz}$) the voltage signal from the accelerometer. The resulting signal was then sampled at a rate of $1000\,\text{Hz}$. The division by 2 and square-root were taken once the signal was discretized.

The temperature of this device had a slight effect on the resonance frequency of the diaphragm. This relationship was determined experimentally by monitoring the temperature of the aluminium retaining ring with an embedded thermocouple. The small, but normal, variation in the ambient temperature during the course of many experiments was recorded and this relationship was then used to correct the final results so that they were more repeatable.

A strict cleaning protocol was used on the upper surface of the diaphragm prior to each run in order to reduce any possible contamination of the free surface of the drop and to promote the repeatability of the results. At the beginning of each set of experiments, an air duster was used to remove any microscopic dust that may have been present on the dry diaphragm. The cleaning procedure used before each individual experiment consisted of the following steps: coarse removal of all secondary droplets with a pipette, drying of the diaphragm surface with a tissue, surface cleaning with acetone, and finally, surface rinsing with distilled water.

A micro-pipette (Eppendorf 200) was used to place varying amounts of distilled water at the centre of the upper surface of the diaphragm in all of these experiments. This micro-pipette has a volume range of 100 to $200\,\mu\text{l}$ and a precision of $0.2\,\mu\text{l}$. The placement of the drops at the centre of the diaphragm was accurate to about $0.5\,\text{mm}$. In addition to sampling the acceleration amplitude, the free-surface motion of the droplet and the evolution of the bursting process were recorded using a Kodak SR-Ultra high-speed video camera with a $1/10\,000\,\text{s}$ shutter speed and a video-framing rate of up to $3000\,\text{fr/s}$.

In its simplest form, the drop-bursting phenomenon is a resonance interaction between the liquid drop as it undergoes droplet ejection and the vibrating diaphragm.
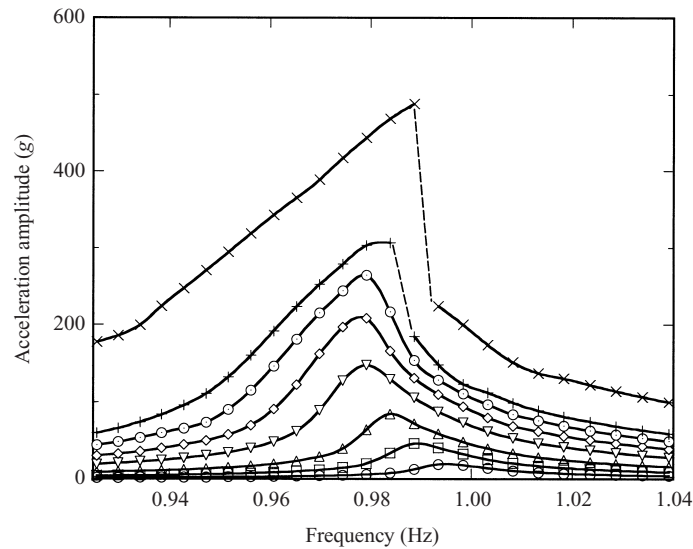
FIGURE 7. Frequency response curves for a dry diaphragm. The applied r.m.s. voltage for each curve is: 0.31 V (○), 0.70 V (□), 1.39 V (△), 2.79 V (▽), 4.18 V (◇), 5.56 V (⊙), 6.93 V (+), and 13.86 V (×). The acceleration amplitude is in g and the frequency is relative to the linear resonance frequency of 982 Hz.

A simple mathematical model for the vibration of a one-degree-of-freedom system, as described in the next section, is capable of duplicating this interaction. To make this model both predictive and faithful with respect to the experimental data, it is necessary to quantify the vibrational characteristics of the dry diaphragm as closely as possible, i.e. accurate values for the stiffness and damping of the diaphragm are needed. The frequency response of a dry diaphragm in terms of its acceleration amplitude for various values of the applied r.m.s. voltage is shown in figure 7.

The behaviour of the diaphragm in the range of very weak to moderate forcing is typical of a slightly soft nonlinear structural member forced near its resonance frequency. As the forcing amplitude increases, the nonlinearity in the system becomes more and more pronounced as evidenced by the change in location of the resonance peak. The resonance frequency first decreases and then increases, indicating that the nonlinearity in the stiffness changes sign. For the highest levels of forcing, the acceleration near resonance appears to have a discontinuity in the frequency response. This is clearly seen in the frequency response curve for the highest voltage level shown in figure 7. As the acceleration magnitude was outside the accelerometer measurement range, this frequency response curve was measured by an optical vibrometer (Polytec 3000; range $= 1500 g$; precision $= 2\%$). Forward and backward frequency sweeps were conducted in this region and hysteresis in the frequency response was not detected. For the remainder of the present work, the experiments were conducted in an acceleration range that excluded this discontinuity. Therefore, drop bursting is not the result of a shock-induced acceleration jump due to the discontinuity seen in figure 7.

4. Mathematical model

A simplified model of the vibrating diaphragm–drop system is shown in figure 8. The diaphragm is modelled as a lumped mass connected to a nonlinear spring, a
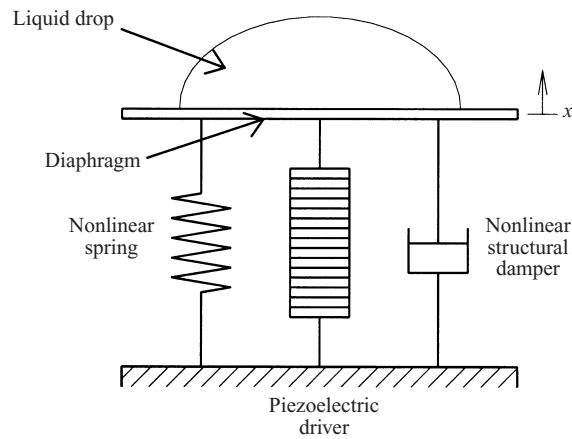
FIGURE 8. A sketch of the mathematical model of the vibrating diaphragm–drop system for VIDA and drop bursting.

nonlinear structural damper, and a piezoelectric ceramic forcing element. The lumped mass includes the mass of the diaphragm, the piezoelectric ceramic, and the attached accelerometer. The generalized mass of these elements is computed based on the measured mode shape of the diaphragm in the frequency range of interest. This computation is discussed in more detail below. The stiffness of the diaphragm is included using a nonlinear spring function fitted to the observed behaviour of a dry diaphragm (figure 7). Nonlinear structural damping is used in this model because the main component of damping in this system is the flexing of the diaphragm itself. The piezoelectric ceramic element is modelled as a linear spring that can vary its length in a linear relation with the applied voltage.†

The liquid drop is also modelled as a generalized lumped mass. This mass is computed by using the actual drop mass, a fixed contact angle, and a spherical-cap shape for the drop. The same vibratory mode shape of the diaphragm that was used for the solid components was also used in this calculation.

Droplet ejection is accounted for by decreasing the liquid-drop mass at a rate that is linearly related to the diaphragm acceleration, if the acceleration is large enough. Otherwise the drop mass remains fixed. A portion of the ejected droplets falls back onto the diaphragm. The contribution of this residual mass to the total generalized mass is computed by assuming that the mass is uniformly distributed on the diaphragm.

For this mathematical model, the displacement of the diaphragm and the varying generalized mass of the liquid drop are described by the following differential equations in time:

$$m\ddot{x} + \frac{c(x)}{\omega}\dot{x} + k(x)x = A\cos(\omega t), \quad x(0) = 0, \quad \dot{x}(0) = 0, \tag{1}$$

$$m = f(m_t, m_d, m_r) \tag{2}$$

$$\dot{m}_d = \begin{cases} 0, & \ddot{x} < a_c \\ -r(\ddot{x} - a_c), & \ddot{x} > a_c, \end{cases} \quad m_d(0) = m_0, \tag{3}$$

$$\dot{m}_r = -p\dot{m}_d, \quad m_r(0) = 0. \tag{4}$$

† (Physik Instrumente GmbH & Co. PI Products for Micropositioning, Catalogue Edition E, CAT.112/D/05.95/13, p. 5.5.)

Here, x is the displacement of the centre of the diaphragm. The total generalized mass of the system, m, is composed of m_t, the mass of the diaphragm, the piezoelectric ceramic, and the attached accelerometer, m_d, the mass of the liquid drop, and m_r, the mass of the residual droplets that have fallen back onto the diaphragm. The nonlinear structural damping of the system is $c(x)$. This form of damping is used in equation (1) (as opposed to viscous damping) because the damping in this system is a result of the flexing of the diaphragm. This flexing motion is why the damping coefficient depends on x, a measure of the deflection of the diaphragm. (See Thomson 1972, §3.10 for an introductory discussion of structural damping.) The nonlinear spring function for the system is $k(x)$, A is the forcing coefficient derived from the piezoelectric ceramic element, and ω is the forcing frequency. Finally, r is the rate of droplet ejection from the primary liquid drop, a_c is the critical acceleration above which droplet ejection occurs, and p is the fraction of ejected droplets that fall back onto the diaphragm. The system is forced with a pure cosine wave. The amplitude of the oscillations of the system is the primary output parameter and so the phase of the forcing signal (sine or cosine) is not important. In addition, the initial transient motion due to the phase of the forcing and the initial conditions occurs over a time scale that is much smaller than the time scale at which mass is lost due to droplet ejection. Thus, these initial transient motions are not important in this study of drop bursting (this statement will be quantitatively supported in §5 using the results plotted in figure 15). The initial drop mass is an important input parameter. However, all of the following simulations were done with $m_0 = 0.2$ g because most of the other system parameters were determined and optimized for this drop mass.

These model equations were designed so that when the acceleration of the diaphragm is less than the critical value, the primary drop mass remains constant, the residual mass remains zero, and the oscillation of the diaphragm is governed by equation (1). In this case, the diaphragm oscillation will reach a periodic state after a short transient period due to the given initial conditions. If the diaphragm acceleration becomes larger than the critical value, the mass of the primary drop decreases due to the ejection of secondary droplets as given by equation (3). This critical value is obtained from experimental observations. Some of the ejected droplets fall back onto the diaphragm. This is modelled by the rate of increase of residual mass given by equation (4). The changes in the primary drop mass and the residual mass affect the total generalized mass of the system through equation (2). (The evaluation of this term is discussed below.) Finally, the changing drop mass modifies the vibration of the diaphragm because it appears in the first term of equation (1). In this case of vibration with droplet ejection the system will also reach a final periodic state. The transient period has a short part due to the given initial conditions and a much longer part due to the mass decrease in the system. This longer transient is the primary interest of the present work.

Equations (1)–(4) were integrated in time using a fourth/fifth-order Runge–Kutta integrator in MATLAB (ode45). To compare the numerical results to the experimental data, the acceleration time response was squared and digitally low-pass-filtered with the same cutoff frequency of 40 Hz as in the experiments. The results were divided by 2, a square-root was taken, and they were then plotted. This procedure converts the high-frequency transient-response acceleration signal to its amplitude. When this amplitude becomes constant the system has reached a periodic state.

The total generalized mass is the sum of the generalized masses of the diaphragm, the piezoelectric ceramic, the attached accelerometer, the primary drop, and the residual droplets. The generalized mass is calculated for each part by integrating the

density of the material over its volume $\mathcal{V}$, weighted by the first axisymmetric mode shape of vibration for the dry diaphragm. The integral is

$$m = \iiint_{\mathcal{V}} \rho \psi^2 \, \mathrm{d}\mathcal{V}. \tag{5}$$

The mode shape, ψ, is a function of the radial position. The generalized mass is an effective mass in which the mass at the centre of the diaphragm, where the diaphragm moves the most, is more heavily weighted than the mass at the edges, where the diaphragm moves only a little. The mode shape was determined experimentally for the unloaded diaphragm driven at 1000 Hz and 0.1 V (r.m.s.). It is scaled to be 1 at the centre. This shape was used to determine all the components of the generalized mass, even when the diaphragm is loaded and the forcing parameters are different. This is justified because the forcing frequencies considered are all close enough to 1000 Hz that the same axisymmetric mode shape of the diaphragm will be excited. Although loading the diaphragm by placing a drop on it will modify the mode shape, and increasing the forcing voltage will increase the amplitude of other modes, these effects were neglected in this simple model.

The generalized masses of the diaphragm, the piezoelectric ceramic, and the attached accelerometer are constants. They were computed using equation (5) with their known geometries and densities. The generalized mass of the primary drop is a function of its actual mass and the drop shape. Here, the drop was assumed to have the shape of a spherical cap with a contact angle of 70°. This value of the contact angle was estimated from the drop image shown in figure 1(*a*). The spherical-cap shape is an approximation, but it is sufficient for the accuracy required in the present model. The generalized mass of the residual droplets is also a function of their mass and distribution. The residual droplets are assumed to be uniformly distributed over the diaphragm and so the integration volume is just a uniform layer covering the extent of the diaphragm. Part of the diaphragm is still covered by the primary drop, so the part of the residual mass that corresponds to this region could be thought of as falling back into the primary drop. The main drawback of this model of the residual mass is that it does not allow this mass to fall back into the primary drop and to be ejected again. Because of this, the model does not capture all of the features of the response that are seen experimentally, as will be discussed in the next section. However, the incorporation of the residual mass into the model does allow for some redistribution of the liquid on the diaphragm, as was observed in the experiments.

The functions used for the nonlinear damping and stiffness are

$$c(x) = c_1 - c_2 \exp(-c_3 x^2), \tag{6}$$

$$k(x) = k_1 + k_2 \exp(-k_3 x^2). \tag{7}$$

These functions, including the values of the constants, were determined to fit the steady-state response of the system computed by the model to the response seen experimentally for an unloaded dry diaphragm. The forcing coefficient, $A = p_f V$, is directly proportional to the amplitude of the forcing voltage, V. The proportionality constant, p_f, was also chosen to fit the model to this data. The experimental data used to do the fitting, and the corresponding results from the model are shown in figure 9. In this figure, the steady-oscillation acceleration amplitude of the diaphragm is plotted as a function of the forcing frequency for three forcing voltages. The experimental data are shown by the symbols. The model results are shown by the solid lines. There is good agreement between the model and the data, indicating that the stiffness
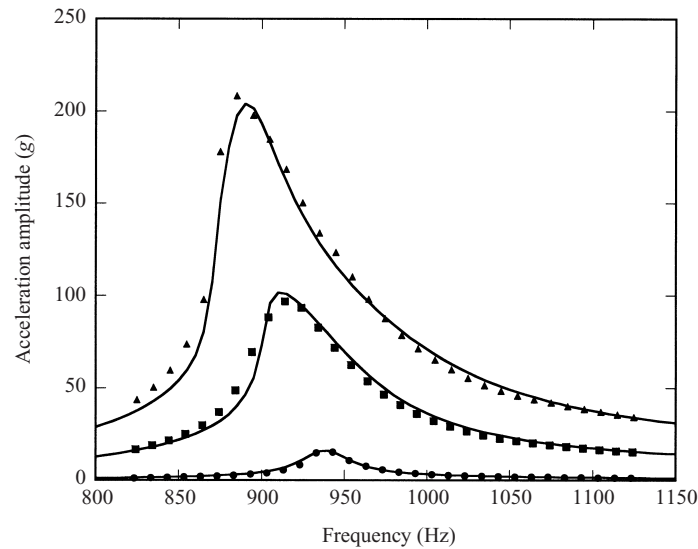
FIGURE 9. A comparison of the results from the mathematical model to the experimental data for an unloaded dry diaphragm with three r.m.s. voltage values: 0.16 V (●), 1.85 V (■), and 4.06 V (▲). The solid lines are the results from the model and the symbols are the experimental data. The linearized resonance frequency of the unloaded diaphragm–drop system is about 982 Hz when more low-voltage data are used to extrapolate down to zero voltage.

and damping functions and all other associated parameters that were chosen for the model provide a reasonable representation of the material characteristics and behaviour of the unloaded diaphragm in this range of forcing parameters. When the forcing voltage is increased further the diaphragm stiffness changes sign and the model predicts the resonance frequency less accurately. The unloaded response outside of this frequency range was not investigated. Placing a liquid drop on the diaphragm modifies the damping and stiffness of the system to a small degree, but these effects were neglected.

The remaining parameters in the model are the droplet-ejection rate, r, the critical acceleration, a_c, and the fraction of ejected droplets that fall onto the diaphragm, p. These parameters were chosen so that the model matched the experimental data for the transient response of the system for a set of cases in which droplet ejection occurred. Four forcing voltages were used, all with a forcing frequency of 1.04 times the initial resonance frequency. The initial resonance frequency is defined to be the resonance frequency of the drop–diaphragm system before any droplet ejection has occurred. The experimental data that were used and the results from the model are given in figure 13, §5. The model parameters were chosen so that the 5.91 V case corresponded correctly to no droplet ejection and the peak amplitudes of the 6.20 and 6.79 V cases occurred close to the correct times.

In summary, a one-dimensional, nonlinear, spring–mass–damper system with a coupled mass-loss function is used to model the diaphragm–drop system and to simulate its response to a piezoelectric driving force. The diaphragm is the oscillator in the model and droplet ejection is modelled with the mass-loss function. Experimental results were used to determine the forms of the stiffness and damping functions and other model parameters by fitting the model simulations to experimental data. The model parameters are held fixed in all the results presented in the next section. The
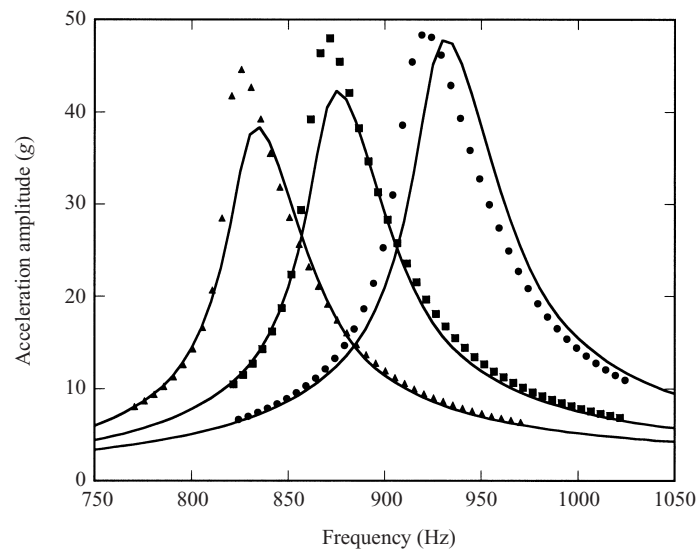
FIGURE 10. The effect of the generalized drop mass on the constant-amplitude oscillation of the diaphragm–drop system without droplet ejection for a 0.74 V (r.m.s.) forcing amplitude. The solid lines are the results from the mathematical model. The symbols are experimental data: 0 g (●), 0.1 g (■), and 0.2 g (▲).

model was designed to be as simple as possible while still capturing the underlying physics and behaviour of the experiments.

To prevent a possible misunderstanding of this model, note that there is a large body of literature in which a spring–mass–damper model is used to simulate the nonlinear dynamics of a dripping faucet. This model was introduced by Shaw (1984) and Martien *et al.* (1985). The difference between that spring–mass–damper model and the one presented here is that the drop-bursting equations (1)–(4) model an oscillating metal diaphragm and its response to the mass loss of a supported liquid drop when droplet ejection begins. The dripping–faucet equations model the oscillation of a liquid drop hanging from a faucet and the response of the drop as fluid is added to it by flow through the faucet. This latter model is used in an attempt to determine the onset of droplet formation and its chaotic behaviour. Both models use similar equations, but the modelled systems are quite different and should not be confused even though droplet formation or ejection is a common event in both situations.

5. Results

The effect of adding a drop to the diaphragm on the constant-amplitude oscillation of the system is shown in figure 10. The constant acceleration amplitude is plotted as a function of the forcing frequency for three cases: the unloaded diaphragm, the diaphragm with a 0.1 g drop (volume = 100 µl), and the diaphragm with a 0.2 g drop (volume = 200 µl). (These mass values are for the generalized drop mass.) The forcing amplitude is 0.74 V (r.m.s.), which is small enough so that droplet ejection does not occur. An increase in the drop mass lowers the resonance frequency and acceleration amplitude of the system.

The mathematical model predicts the decrease in the resonance frequency quite well, but overpredicts the decrease in the peak resonance amplitude. The model peak amplitude is about 14% lower than the experimental peak for the largest drop mass
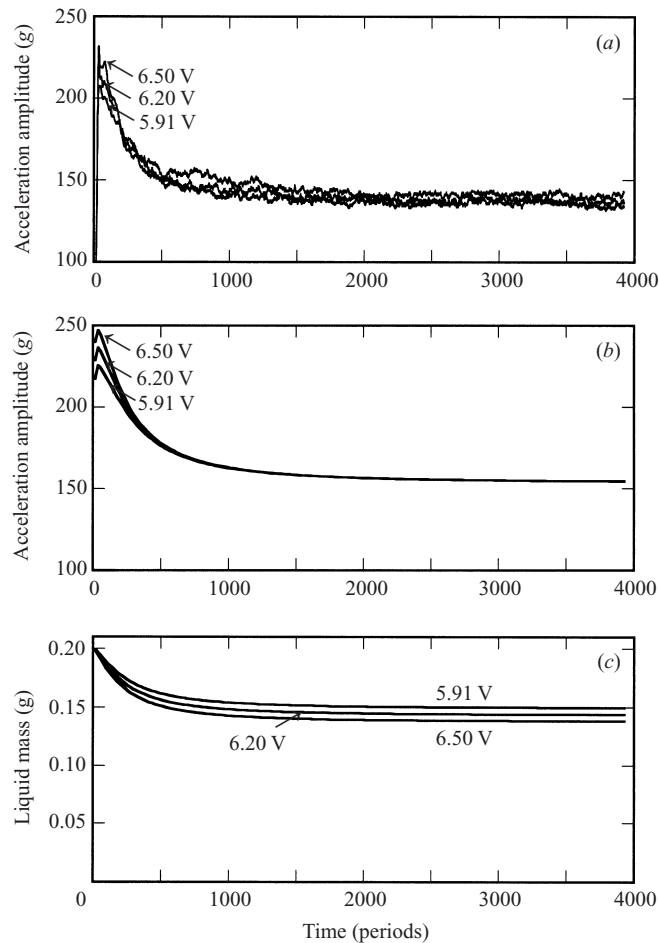
FIGURE 11. The response of the diaphragm–drop system to a forcing frequency of 0.99 times the initial resonance frequency of the system of 785 Hz. The initial drop volume is 200 μl. (*a*) The measured system-acceleration amplitude, (*b*) the simulated system-acceleration amplitude, and (*c*) the simulated generalized mass of the liquid drop.

considered. The discrepancy is primarily due to the fact that the structural parameters for the model were optimized for a system acceleration response of about 100 *g*. The experimental data in figure 10 do not exceed an acceleration of 50 *g* so as to prevent any droplet ejection. Note that when droplet ejection does occur the primary drop mass will decrease and so the resonance frequency of the diaphragm–drop system will increase in time. This dependence of the system resonance frequency on the drop mass is the key to understanding the transient behaviour of the system, particularly the bursting phenomenon.

For the remainder of the results in this section, the initial mass of the drop will be 0.2 g (volume = 200 μl). The transient response of the system is shown in figure 11 for three forcing voltages and a forcing frequency that is 0.99 times the initial resonance frequency of the diaphragm–drop system. Figure 11(*a*) shows the experimentally measured acceleration amplitude, figure 11(*b*) shows the acceleration amplitude computed by the model, and figure 11(*c*) shows the generalized mass of the liquid drop on the diaphragm as computed by the model.
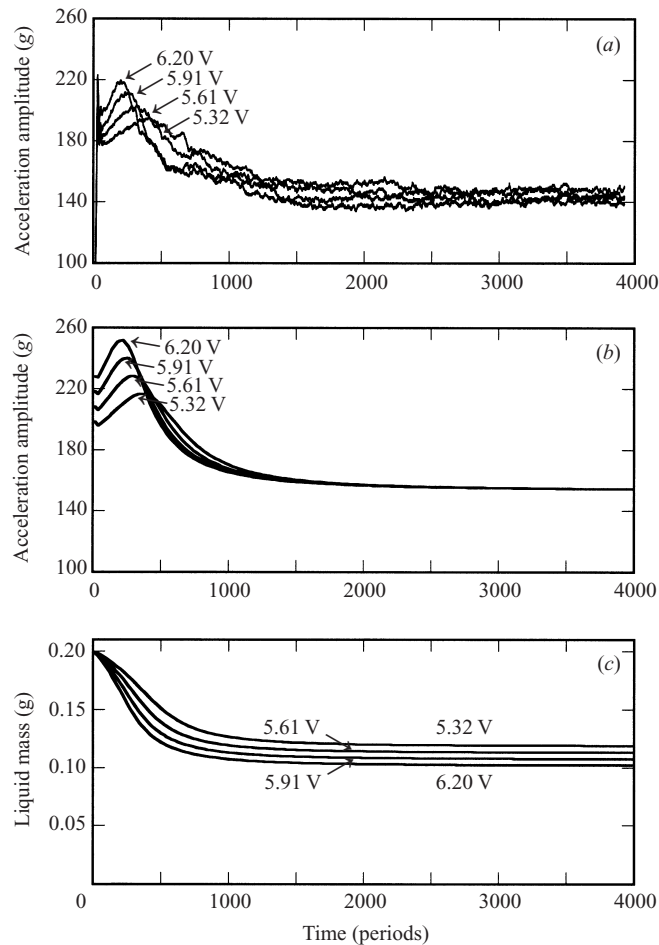
FIGURE 12. As figure 11 but for a forcing frequency of 1.01 times the initial resonance frequency of the system of 785 Hz.

The forcing voltage is turned on at a constant value resulting in a very brief transient during which the system acceleration amplitude jumps above the critical value. Secondary droplets are ejected, the system mass decreases, and the system resonance frequency increases. Since the forcing frequency is less than the initial resonance frequency, the system moves farther away from resonance during this process. This causes the system acceleration to decrease, which in turn causes droplet ejection to slow and eventually to stop. All three cases have essentially the same behaviour except that the larger forcing voltages result in larger initial accelerations and more droplet ejection. All cases reach a constant-amplitude periodic oscillation when the acceleration reaches the critical value, at which time droplet ejection stops. Therefore, all three cases have the same final acceleration amplitude, although the final values of the drop mass are different. Note that although the model somewhat overpredicts the response amplitude, it is in the correct range and the system behaviour is well-captured qualitatively. The liquid mass was not measured in the experiments, except for the initial mass, so the model is useful in providing an idea of the transient variation of the liquid mass.

Similar results are presented in figure 12 for a forcing frequency of 1.01 times the initial resonance frequency of the diaphragm–drop system. Initially, the response
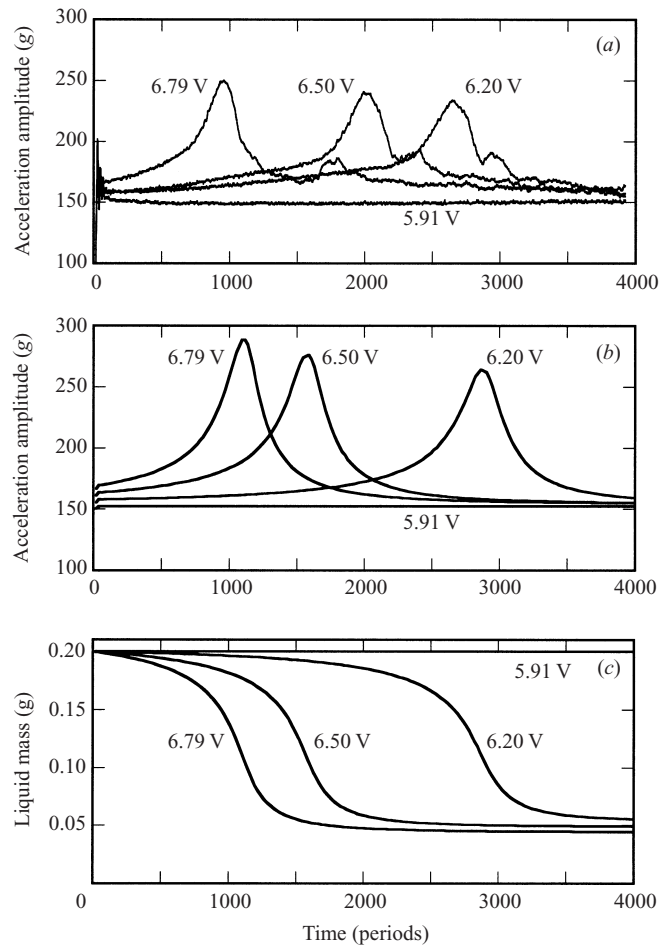
FIGURE 13. As figure 11 but for a forcing frequency of 1.04 times the initial resonance frequency of the system of 785 Hz.

acceleration is above the critical value, so droplet ejection occurs. As in the case shown in figure 11, the system mass decreases and the resonance frequency increases, but now the system moves towards resonance since the forcing frequency was initially above the resonance frequency. This causes the acceleration amplitude to increase and the droplet-ejection rate to increase. This continues until the system reaches the resonance condition and the acceleration reaches a maximum. After this the system moves away from resonance, the system acceleration decreases, and droplet ejection slows and finally stops. The drop may appear to be bursting as the system moves towards resonance and the droplet-ejection rate increases, if the forcing voltage is large enough. In such cases, the system reaches resonance more quickly, as indicated by the earlier location of the acceleration peaks in figures 12(*a*) and 12(*b*). However, the drop does not completely burst since there is still more than half of the initial drop mass left on the diaphragm when the system finally reaches a constant oscillation amplitude. The amplitudes of the peak accelerations are overpredicted by the model by no more than 15%.

Figure 13 is the one case where the critical acceleration for droplet ejection and the droplet-ejection rate parameters were chosen to best fit the data. Here, the forcing

frequency is 1.04 times the initial resonance frequency of the diaphragm–drop system. At this higher initial frequency, it takes longer for the system to reach the resonance peak and the peak accelerations for the different driving voltages are more spread out in time.

Since the system starts farther from resonance the initial acceleration and droplet-ejection rate are smaller. As seen in figure 13(*c*), the speeding up and then slowing down of droplet ejection is more pronounced than in the previous case, and the drop loses about 75% of its initial mass. For the lowest forcing-amplitude case, the acceleration does not exceed the critical value and so droplet ejection does not occur, as intended. As in the previous two cases, the model overpredicts the system-response acceleration by at most 16%.

The experimental system-acceleration amplitude traces of figure 13(*a*) and the simulated traces of figure 13(*b*) are the signatures of drop bursting. Visually, the drop surface is in a state of very chaotic wave motion, like that seen in figure 1(*e*). Then droplet ejection begins and, quite suddenly, the drop bursts into a spray of smaller secondary drops. When the spray disappears, only a much smaller drop remains on the diaphragm along with some residual secondary droplets that have fallen back onto that surface.

In figure 13(*a*), the three cases in which droplet ejection occurs have a second, smaller peak in amplitude after the first one. This peak occurs for other forcing frequencies as well, although it is less pronounced. This small peak is due to the behaviour of the ejected secondary droplets. Droplets that fall back on the primary drop eventually coalesce with it, and some of the droplets that fall on the diaphragm tend to travel toward the centre of the diaphragm and coalesce with the primary drop. These events increase the generalized mass of the system, which decreases the resonance frequency and brings the system back towards resonance. Thus, the system-response amplitude and the droplet-ejection rate increase. This event appears as a second burst of the primary drop, although it is not as vigorous or as large as the first one. This phenomenon is not captured by the mathematical model because the model does not allow for any movement or coalescence of the secondary droplets with the primary drop. The secondary droplets are assumed to land on the diaphragm uniformly and to stay where they are. However, the understanding of the initial burst, as gained from the model, along with the observation that the residual droplets do travel to the centre of the diaphragm and coalesce with the primary drop leads naturally to this explanation of the second mini-burst.

One advantage of the mathematical model is that it allows the simulation of the system response in parameter ranges that are out of reach experimentally. For instance, figure 14 shows the system response for forcing voltages of 20 and 40 V (r.m.s.) and a forcing frequency 1.13 times the initial resonance frequency. (Note: while such large voltages could be applied to the transducer, the resulting motion of the diaphragm would be so large that the piezoelectric ceramic could delaminate or crack. Thus, 25 V was used as the maximum allowed forcing voltage in these experiments in order to prevent any accidental damage to the transducer.) In both cases, droplet ejection begins immediately and the system moves closer to resonance as the resonance frequency of the system increases. However, before the acceleration amplitude reaches the resonance peak, the drop mass becomes zero as shown in figure 14(*b*). With no more liquid to eject, the diaphragm just continues to vibrate in this state of high-amplitude acceleration as seen in figure 14(*a*). These two events are examples of instantaneous drop bursting. Figure 2 shows an experimental visualization of such an event, although not at such large forcing voltages.
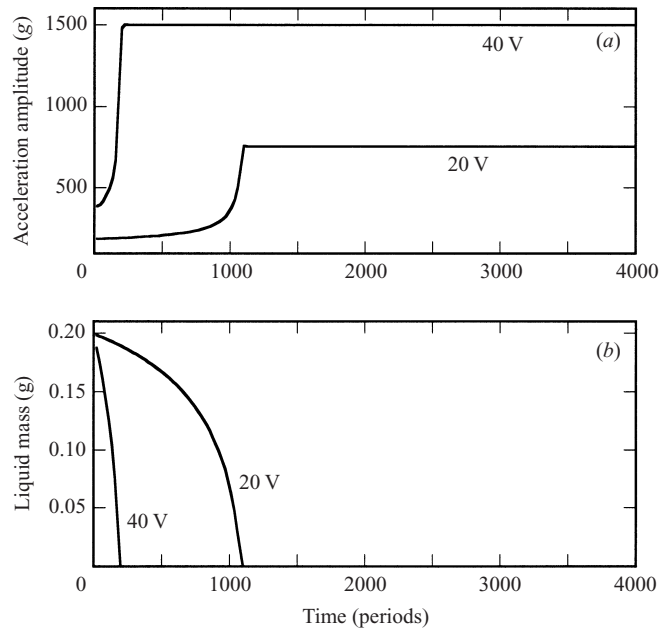
FIGURE 14. The response of the diaphragm–drop system to a forcing frequency of 1.13 times the initial resonance frequency and for two very large forcing voltages. The initial drop volume is 200 μl. (*a*) The simulated system-acceleration amplitude, and (*b*) the simulated generalized mass of the liquid drop.

In figure 15, the system response is presented in a different way. The transient system-acceleration amplitude is cross-plotted as a function of the generalized mass of the liquid drop, with time as a varying parameter along each curve. The experimental transient results of figures 13(*b*) and 13(*c*) are shown by the symbols for three forcing voltages. In each case, a symbol represents one instant in time, with time increasing from right to left. The forcing frequency is 1.04 times the initial resonance frequency of the diaphragm–drop system. The data represented by the lines were computed by setting the droplet-ejection rate to zero, fixing the drop mass, fixing the forcing parameters, and calculating the acceleration amplitude of the final constant-amplitude oscillation. This gives the response of the system to the forcing without any droplet ejection. The excellent agreement between the transient data (the symbols) and the constant-amplitude oscillation data (the lines) shows that the transient acceleration response is quasi-steady. This is expected since the time scale for the droplet-ejection response is about 100 to 1000 times the time scale for the system oscillations themselves.

6. Discussion

The VIDA bursting phenomenon examined in the previous section has two essential components. The first is the purely fluid-dynamical process of capillary wave motion that forms on the free surface of the drop and its consequences. As the forcing amplitude increases, these waves develop in a complex manner, interact with each other, and finally lead to the formation of a crater and then an intense liquid jet. At the tip of the jet a droplet forms, pinches off, and is ejected from the primary drop. The details of this part of the bursting phenomenon, as shown in figures 3–5, is examined in James *et al.* (2003).
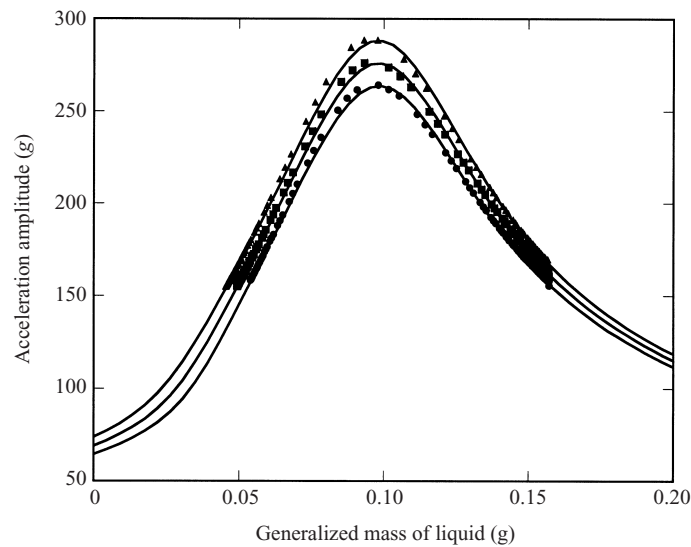
FIGURE 15. A comparison of the simulated constant-amplitude oscillation response of the system (solid lines) and the simulated transient response (symbols) for a forcing frequency of 1.04 times the initial resonance frequency of the diaphragm–drop system of 732 Hz, and for three r.m.s. voltages: 6.20 V (●), 6.50 V (■), and 6.79 V (▲).

The second component of drop bursting is the fluid/structure interaction process in which the vibrating diaphragm interacts with the fluid drop mass that sits on it and that varies as droplet ejection occurs. The final goal of the present paper is to clearly explain this fluid/structural-dynamics process through which drop bursting takes place.

To simplify the following discussion and to clearly demonstrate the basic physics of the drop bursting process, the mathematical model presented in §4 is revisited and four additional simplifications are made. First, note that there are two distinct time scales in this problem. The first is the time period of the forced oscillations, which is in the neighbourhood of $\tau_f = 1$ ms for driving frequencies near 1000 Hz. The second time scale, τ_d, is the time over which the atomization process occurs. Based on experimental results, $\tau_f \ll \tau_d$. This result is also proven by the data plotted in figure 15. A formal multi-scale analysis of equations (1)–(4) leads to the conclusion that the structural-vibration equation (1) decouples from the mass-loss equation based on droplet ejection (3). Thus, one can solve for the constant-amplitude oscillations of the diaphragm with a fixed drop mass first and then input this result directly into the drop-mass-loss equation afterwards. Following this formal separation, the resulting oscillation equation is solved with two further simplifications. First, the system is linearized by using constants for the stiffness and the structural damping coefficients of the diaphragm. Second, all transient oscillations in the diaphragm are ignored and only the steady-state oscillation amplitude is computed. As a result of these simplifications, the constant acceleration amplitude of the oscillations of the diaphragm is given by

$$a = p_f V \omega^2 [(k - m\omega^2)^2 + c^2]^{-1/2}. \tag{8}$$

This equation shows that the acceleration amplitude goes to zero as the driving frequency goes to zero and it approaches a constant as the driving frequency becomes
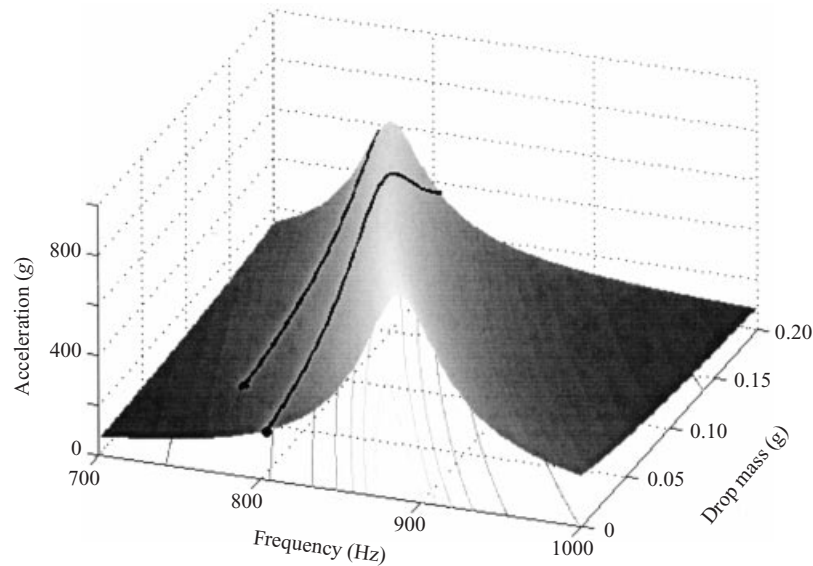
FIGURE 16. A surface plot of the acceleration amplitude for the linear drop–diaphragm system driven at 12 V (r.m.s.). The two black lines show the time history of the system driven at 765 Hz and 804 Hz. The time is zero at the top of the black curves (drop mass = 0.2 g) and increases as one moves down the curves toward a zero drop mass. The resonance frequency for the unloaded diaphragm is 887 Hz and for the fully loaded system it is 773 Hz.

large. There is also a resonance peak that is shown in figure 16 as a surface whose elevation is the system-acceleration amplitude as a function of the driving frequency and the generalized mass of the primary drop. This figure shows that as the drop mass increases the system resonance frequency decreases, as expected. This result is also seen in the experiments and the full simulations shown in figure 10.

The time history of the drop mass during droplet ejection caused by this acceleration amplitude was found by integrating the droplet-ejection equation (3) along with the acceleration-amplitude equation (8). The same MATLAB integration routine was used as before, ode45. The fourth and final simplification is to ignore the secondary droplets that fall back on the diaphragm by ignoring the residual droplet equation (4). Two computed trajectories with different frequencies, but with the same driving voltage are plotted in figure 16. Each of these trajectories starts with the diaphragm fully loaded with a primary drop of generalized mass 0.2 g. Note that for the purposes of this discussion, the diaphragm is considered fully loaded whenever the 0.2 g drop is present. However, this is just a convenience and the arguments presented in this section hold equally well if a different initial drop mass is used. In figure 16, two system trajectories are shown: one has a driving frequency less than the fully loaded diaphragm resonance frequency and the other has a driving frequency greater than the fully loaded diaphragm resonance frequency. The trajectories start at a drop mass of 0.2 g and end at the small black filled circles. The curve for the lower frequency shows that the diaphragm acceleration amplitude steadily decreases until the system reaches the critical acceleration for droplet ejection. At this point, the diaphragm continues to vibrate with a much smaller drop on its surface. While there was droplet ejection, there was no bursting. The acceleration never reached a large maximum because the driving frequency was less than the resonance frequency and always decreased. At the higher driving frequency, the trajectory of the system passes through an acceleration
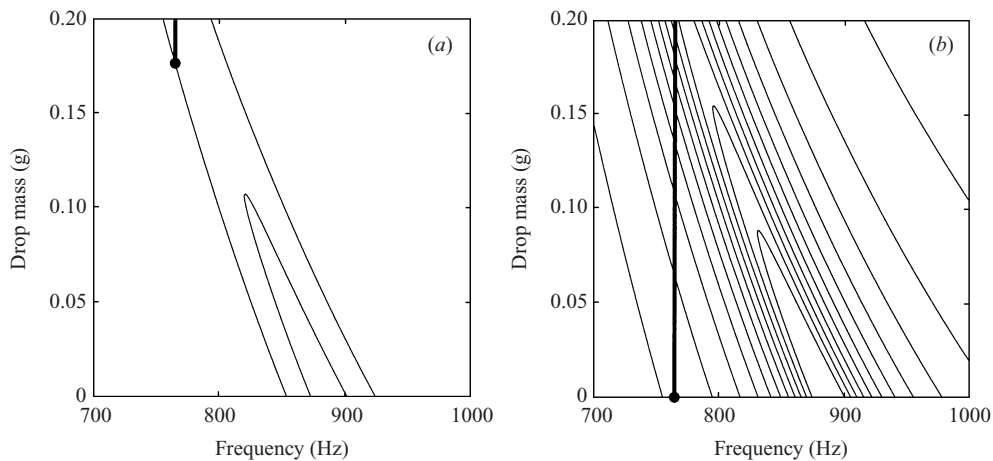
FIGURE 17. (*a*) System-acceleration amplitude contours for the low-voltage case of 4 V (r.m.s.). (*b*) System-acceleration amplitude contours for the high-voltage case of 16 V (r.m.s.). The outer contours in each plot are the contours for 152 g, the threshold for droplet ejection. The driving frequency for both cases is 765 Hz, a frequency 0.99 times the loaded diaphragm–drop resonance frequency. The increment between successive contour lines is 80 g.

maximum, causing a rapid burst, and then continues to eject secondary droplets until the entire initial drop has been removed from the diaphragm.

Another way to visualize these data is to replot equation (8) as a contour plot in frequency and drop mass as shown in figure 17. Now, consider two cases in which the driving frequency is less than the fully loaded diaphragm resonance frequency and the driving voltage is large enough to cause droplet ejection. The dynamics of the diaphragm–drop system can be determined by following the two vertical lines in figure 17 straight down until they stop at the small black filled circles. The plots show that both the mass of the drop and the system acceleration amplitude monotonically decrease until the acceleration reaches the critical amplitude for droplet ejection (figure 17*a*) or until the drop mass has all been ejected (figure 17*b*). The system then vibrates unchanged and the mass of the drop stays constant or it is not present. This is quantified in the time-history plots of drop mass and system-acceleration amplitude shown in figure 18. For both cases, the mass of the drop and the system-acceleration amplitude monotonically decrease. However, in the high-voltage case there is enough droplet ejection to completely remove the drop from the diaphragm and then the diaphragm continues to vibrate with an acceleration amplitude that is higher than the critical acceleration. For the low-voltage case, droplet ejection occurs until the system reaches the critical acceleration amplitude for droplet ejection (152 g). After this, the drop–diaphragm system continues to oscillate at that acceleration level. In each case, this monotonically decreasing mass loss is not a bursting event, although it is still VIDA.

Next, consider two cases in which the driving frequency is greater than the fully loaded diaphragm resonance frequency. The dynamics for these cases are shown in the contour plots of figure 19 and the associated time-history plots of figure 20. For the lowest-voltage case, the system-acceleration amplitude starts at 150 g, just below the critical acceleration for droplet ejection, and so the system vibrates with a constant acceleration amplitude and there is no droplet ejection (figure 20*a*, *b*). For the second lowest-voltage case, the system acceleration starts at 153 g, just above
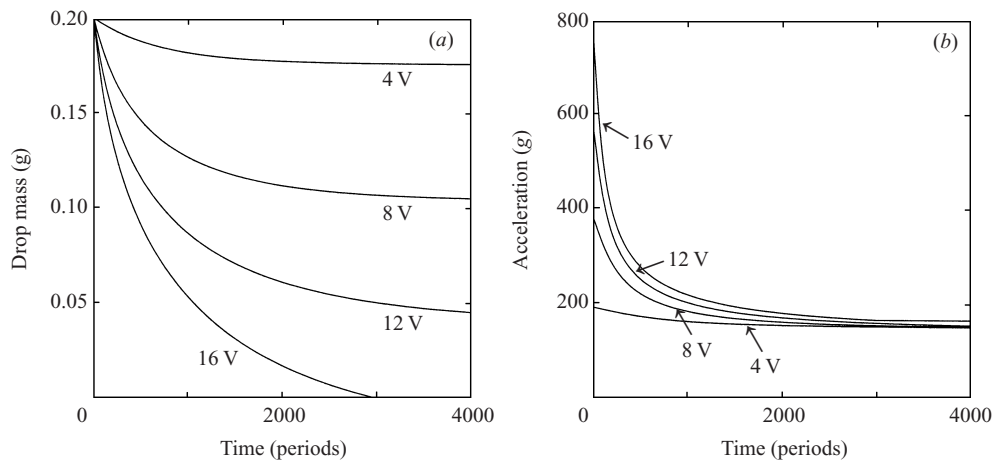
FIGURE 18. (*a*) The time history of the drop mass with time measured in periods of the forcing frequency for four different voltages. (*b*) The time history of the drop–diaphragm system-acceleration amplitude in units of *g* with time measured in periods of the forcing frequency for four different voltages. The driving frequency for all cases is 765 Hz, a frequency 0.99 times the fully loaded diaphragm–drop resonance frequency.

the critical acceleration (figure 19*a*). The system vibrates and there is a slow mass loss due to droplet ejection as shown in figure 20(*a*). As the mass decreases, the system resonance frequency increases toward the driving frequency and the amplitude of the oscillations increases. In time, the system moves rapidly through resonance and attains the highest acceleration and the fastest mass loss possible. This rapid droplet ejection is the signature of a bursting event. For this voltage, 90% of the drop mass is lost during the crossing of the resonance peak over a time period of about 2.5 s. After the burst, the mass and acceleration amplitude continue to decrease until the acceleration amplitude reaches the critical value. After this time, the diaphragm continues to vibrate at the critical acceleration amplitude with a smaller primary drop remaining on its surface.

In the high-voltage case, the result is similar. The difference is that the acceleration amplitude starts at a higher value. Thus, the rate of droplet ejection is higher initially and the crossing of the resonance acceleration amplitude peak occurs earlier and it is faster. Here, 90% of the drop mass is ejected in about 1.2 s. After about another 0.5 s, the entire drop mass is gone and the system stays at a constant acceleration amplitude of 194 *g*, well above the critical value of 152 *g*.

A comparison of the results of the linear model of figure 20(*b*) to those of the full nonlinear coupled model given in figure 13(*b*) and the experimental results of figure 13(*a*) shows that the linear model has captured the essence of the drop-bursting process. Notice though that the linear model is much less sensitive to the driving voltage than either the nonlinear model or the experiments. Despite this loss of sensitivity, the linear model is a simple way to demonstrate that VIDA drop bursting is an unusual resonance phenomenon in which the driving frequency is fixed above the resonance frequency of the system and the mass loss due to droplet ejection causes the system to move through its resonance frequency. In doing so, the system undergoes a rapid increase in droplet ejection in which the drop appears to burst or explode into a spray of smaller secondary droplets. At the end of this process, the drop has either completely disappeared or else there is a very small drop left to vibrate on the diaphragm.
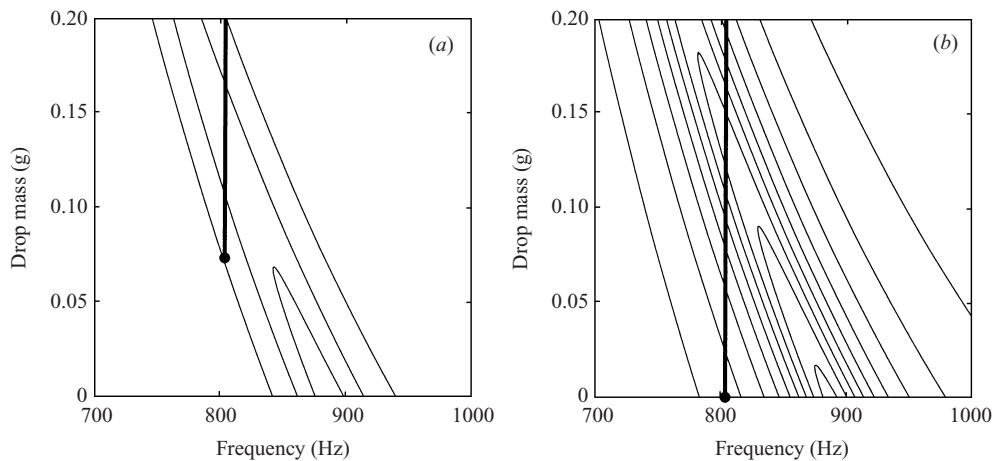
FIGURE 19. (*a*) System-acceleration contours for the low-voltage case of 5.1 V (r.m.s.). (*b*) System-acceleration contours for the high-voltage case of 12 V (r.m.s.). The outer contours in each plot are the contours for 152 *g*, the threshold for droplet ejection. The driving frequency for both cases is 804 Hz, a frequency 1.04 times the loaded diaphragm–drop resonance frequency. The increment between successive contour lines is 80 *g*.

7. Conclusions

This paper has introduced and characterized a new atomization process called vibration-induced drop atomization (VIDA) and a dramatic companion event called drop bursting. The bursting process combines the fluid dynamics of droplet ejection from a vibration-induced jet emanating from the free surface of a liquid drop and the dynamics of a vibrating drop–diaphragm system. Bursting occurs when the driving frequency is above the initial resonance frequency of the drop–diaphragm system and the driving voltage is above a critical value for droplet ejection. The mass loss due to droplet ejection continually increases the system resonance frequency until it equals the driving frequency. Naturally, this results in a resonance event in which the acceleration amplitude of the oscillations becomes very large. This makes the droplet-ejection rate so large that the drop appears to burst or explode into a spray of small secondary droplets. After bursting, if some of the liquid drop remains on the diaphragm, the system continues to oscillate with decreasing amplitude and the droplet-ejection rate decreases. The event stops when either the initial drop has disappeared or the system-acceleration amplitude reaches the critical acceleration amplitude for droplet ejection.

If the driving frequency is above the system resonance frequency and the initial system-acceleration amplitude is high enough, the rate of droplet ejection will be very large and the drop may appear to burst immediately. The time delay for the bursting event depends on two parameters: the difference between the initial system-acceleration amplitude and the critical acceleration amplitude; and the difference between the driving frequency and the initial system resonance frequency. As the acceleration difference decreases, the time delay for bursting to occur increases. This is illustrated explicitly in the experimental results (figure 13*a*), the results from the nonlinear mathematical model (figure 13*b*), and the results from the simple linear model (figure 20*b*). When the frequency difference decreases, the time delay for bursting also decreases. This is illustrated in the experimental results of figures 12(*a*) and 13(*a*) and the numerical results of figures 12(*b*) and 13(*b*).
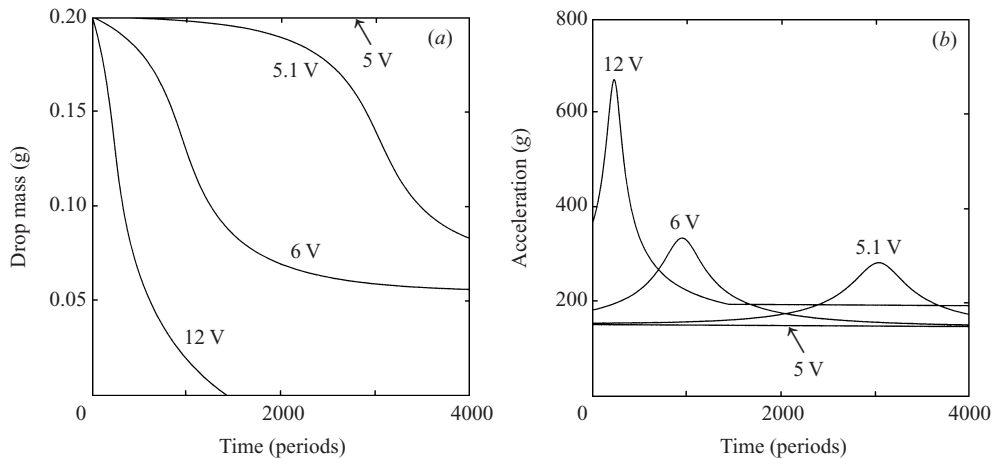
FIGURE 20. (*a*) The time history of the drop mass with time measured in periods of the forcing frequency for four different voltages. (*b*) The time history of the drop–diaphragm system-acceleration amplitude in units of g with time measured in periods of the forcing frequency for four different voltages. For the 5 V (r.m.s.) case, the system is vibrating at $150\,g$, which is below the critical acceleration level of $152\,g$, and so there is no droplet ejection. The driving frequency for all cases is 804 Hz, a frequency 1.04 times the fully loaded diaphragm–drop resonance frequency.

If the driving frequency is set below the system resonance frequency and the initial system-acceleration amplitude is above the critical acceleration amplitude for droplet ejection then all one sees is a steadily decreasing rate of droplet ejection until either the initial drop has disappeared or the system-acceleration amplitude reaches the critical value for droplet ejection. The process is still droplet atomization or VIDA, but it is not a bursting event as defined in this paper.

The experiments described in §3 and the visualizations shown in §2 dramatically demonstrate that the VIDA-bursting process and the nonlinear mathematical model discussed in §4 have successfully isolated the essential physics of the process. The mathematical model has several drawbacks though. Its parameters and the stiffness and damping functions were chosen to fit the model results to the experimental results for a particular piezoelectric diaphragm and for a particular liquid, i.e. water. Also, some of the assumptions used in constructing the mathematical model may not be exactly correct. For example, the work of Goodridge *et al.* (1997) suggests that the critical acceleration is a function of the forcing frequency. This dependence was not included in this model. Despite these shortcomings, the nonlinear mathematical model has served the purpose of helping to elucidate the behaviour and physics of VIDA and the drop-bursting process. This is made very clear in the success of the linear bursting model of §6 in mimicking the effects seen in experiments.

The key to the VIDA process and especially to the VIDA drop-bursting event investigated here is the use of a vibrating diaphragm driven by an integrated piezo-electric actuator. This low-mass device yields acceleration amplitudes well above the $150\,g$ level that are needed to eject small secondary droplets from the larger drop and even from a thin liquid film at the ejection rates that are the hallmark of VIDA. It is possible to produce the VIDA effect with a stiff driver (e.g. a mechanical shaker) if it could reach the required acceleration levels. Mechanical shakers that can attain these acceleration levels require high-power levels, and are large and expensive. In contrast, piezoelectric actuators require low-power levels, and are small and inexpensive.

Finally, a series of experiments and numerical studies are underway that will yield a detailed understanding of the process through which individual droplets are ejected from a free-surface wave crest. The numerical work of James *et al.* (2003) uses a VOF method to compute the motion and deformation of the vibrating drop all the way to droplet ejection. Related experiments by Range, Glezer & Smith (2003) use a mechanical shaker to look at droplet ejection from single small sessile drops. This kind of detailed information is needed in order to determine the critical acceleration and the rate of droplet ejection used in the nonlinear system model described above. Attaining this level of understanding of the droplet-ejection process will allow the optimization of VIDA technology for use in many different kinds of engineering systems.

There are many potential uses of the VIDA process and current research is exploring several. VIDA bursting is effective for spray cooling of microprocessors and spray coating of a solid surface. It may be effective to use this process for the atomization of fuel for spray-injection nozzles, as a fluid-emulsification system, and for droplet encapsulation of time-released drug-delivery systems.

REFERENCES

BASARAN, O. A. & DEPAOLI, D. W. 1994 Nonlinear oscillations of pendant drops. *Phys. Fluids* **6**, 2923–2943.

BENJAMIN, T. B. & URSELL, F. 1954 The stability of the plane free surface of a liquid in vertical periodic motion. *Proc. R. Soc. Lond.* A **225**, 505–515.

CILIBERTO, S. & GOLLUB, J. P. 1985 Chaotic mode competition in parametrically forced surface waves. *J. Fluid Mech.* **158**, 381–398.

DECENT, S. P. & CRAIK, D. D. 1995 Hysteresis in Faraday resonance. *J. Fluid Mech.* **293**, 237–268.

DEPAOLI, D. W., SCOTT, T. C. & BASARAN, O. A. 1992 Oscillation frequencies of droplets held pendant on a nozzle. *Separation Sci. Tech.* **27**, 2071–2082.

EDGERTON, H. E. & KILLIAN, J. R. 1939 *Flash! Seeing the Unseen by Ultra High-Speed Photography.* Boston: Hale, Cushman, & Flint.

EDWARDS, W. S. & FAUVE, S. 1994 Patterns and quasi-patterns in the Faraday experiment. *J. Fluid Mech.* **278**, 123–148.

FARADAY, M. 1831 On the forms and states assumed by fluids in contact with vibrating elastic surfaces. *Phil. Trans. R. Soc. Lond.* **52**, 319–340.

FUKAI, J., SHIIBA, Y., YAMAMOTO, T., MIYATAKE, O., POULIKAKOS, D., MEGARIDIS, C. M. & ZHAO, Z. 1995 Wetting effects on the spreading of a liquid droplet colliding with a flat surface: experiment and model. *Phys. Fluids* **7**, 236–247.

GAÑÁN, A. & BARRERO, A. 1990 Free oscillations of liquid captive drops. *Microgravity Sci. Technol.* III **2**, 70–86.

GIAVEDONI, M. D. 1995 A numerical study of the two-dimensional dynamic behavior of a thin liquid film subject to a vertical oscillation. *Ind. Engng Chem. Res.* **34**, 356–365.

GOODRIDGE, C. L., SHI, W. T., HENTSCHEL, H. G. E. & LATHROP, D. P. 1997 Viscous effects in droplet-ejecting capillary waves. *Phys. Rev.* E **56**, 472–475.

JAMES, A., SMITH, M. K. & GLEZER, A. 2003 Vibration-induced drop atomization and the numerical simulation of low-frequency single-droplet ejection. *J. Fluid Mech.* **476**, 29–62.

JIANG, L., PERLIN, M. & SCHULTZ, W. W. 1998 Period tripling and energy dissipation of breaking standing waves. *J. Fluid Mech.* **369**, 273–299.

JIANG, L., TING, C.-L., PERLIN, M. & SCHULTZ, W. W. 1996 Moderate and steep Faraday waves: instabilities, modulation and temporal asymmetries. *J. Fluid Mech.* **329**, 275–307.

KUMAR, K. & TUCKERMAN, L. S. 1994 Parametric instability of the interface between two fluids. *J. Fluid Mech.* **279**, 49–68.

Lee, C. P., Anilkumar, A. V. & Wang, T. G. 1991 Static shape and instability of an acoustically levitated drop. *Phys. Fluids* A **3**, 2497–2515.

Martien, P., Pope, S. C., Scott, P. L. & Shaw, R. S. 1985 The chaotic behavior of the leaky faucet. *Phys. Lett*. A **110**, 399–404.

Miles, J. 1993 On Faraday waves. *J. Fluid Mech.* **248**, 671–683.

Miles, J. & Henderson, D. 1990 Parametrically forced surface waves. *Annu. Rev. Fluid Mech.* **22**, 143–165.

Nayfeh, A. H. & Nayfeh, J. F. 1990 Surface waves in closed basins under principal and autoparametric resonances. *Phys. Fluids* A **2**, 1635–1648.

Newitt, D. M., Dombrowski, N. & Knelman, F. H. 1954 Liquid entrainment. 1. The mechanism of drop formation from gas or vapour bubbles. *Trans. Inst. Chem. Engrs* **32**, 244–261.

Oguz, H. N. & Prosperetti, A. 1990 Bubble entrainment by the impact of drops on liquid surfaces. *J. Fluid Mech.* **219**, 143–179.

Pumphrey, H. C. & Crum, L. A. 1988 Acoustic emissions associated with drop impacts. In *Sea Surface Sound* (ed. B. R. Kerman), pp. 463–483. Kluwer.

Pumphrey, H. C., Crum, L. A. & Bjørnø, L. 1989 Underwater sounds produced by individual drop impacts and rainfall. *J. Acoust. Soc. Am.* **85**, 1518–1526.

Range, K., Glezer, A. & Smith, M. K. 2003 Vibration-induced drop ejection from sessile drops. *In preparation.*

Rodot, H., Bisch, C. & Lasek, A. 1979 Zero-gravity simulation of liquids in contact with a solid surface. *Acta Astronautica* **6**, 1083–1092.

Shaw, R. 1984 *The Dripping Faucet as a Model Chaotic System.* Santa Cruz, CA: Aerial Press.

Smith, M. K., James, A., Vukasinovic, B. & Glezer, A. 1998 Vibration-induced droplet atomization. *Proc. Fourth Microgravity Fluid Physics and Transport Phenomena Conference, Cleveland, OH*, pp. 447–452.

Snyder, H. E. & Reitz, R. D. 1998 Direct droplet production from a liquid film: a new gas-assisted atomization mechanism. *J. Fluid Mech.* **375**, 363–381.

Sorokin, V. I. 1957 The effect of fountain formation at the surface of a vertically oscillating liquid. *Akust. Zh.* **3**, 281–291.

Strani, M. & Sabetta, F. 1984 Free vibrations of a drop in partial contact with a solid support. *J. Fluid Mech.* **141**, 233–247.

Strani, M. & Sabetta, F. 1988 Viscous oscillations of a supported drop in an immiscible fluid. *J. Fluid Mech.* **189**, 397–421.

Thomson, W. T. 1972 *Theory of Vibration with Applications.* Prentice-Hall.

Vukasinovic, B., Glezer, A. & Smith, M. K. 2000 Vibration-induced droplet atomization. *Phys. Fluids* **12**, S12.

Vukasinovic, B., Glezer, A. & Smith, M. K. 2001 Mode shapes of a sessile drop in forced vibration. *Phys. Fluids* **13**, S14.

Wilkes, E. D. & Basaran, O. A. 1997 Forced oscillations of pendant (sessile) drops. *Phys. Fluids* **9**, 1512–1528.

Wilkes, E. D. & Basaran, O. A. 1998 Drop ejection from an oscillating rod. *Proc. Fourth Microgravity Fluid Physics and Transport Phenomena Conference*, Cleveland, OH, pp. 540–545.

Wilkes, E. D. & Basaran, O. A. 2001 Drop ejection from an oscillating rod. *J. Colloid Interface Sci.* **242**, 180–210.

Woods, D. R. & Lin, S. P. 1995 Instability of a liquid film flow over a vibrating inclined plane. *J. Fluid Mech.* **294**, 391–407.

Yule, A. J. & Al-Suleimani, Y. 2000 On droplet formation from capillary waves on a vibrating surface. *Proc. R. Soc. Lond.* A **456**, 1069–1085.

Zhang, W. & Vinals, J. 1997 Pattern formation in weakly damped parametric surface waves. *J. Fluid Mech.* **336**, 301–330.